ChemPubSoc Europe

DOI: 10.1002/batt.201800091

BATTERIES & SUPERCAPS Communications

Ultra-Thin Coating and Three-Dimensional Electrode Structures to Boosted Thick Electrode Lithium-Ion Battery Performance

Jie Li,[a] Yan Gao,[b] Xinhua Liang,[b] and Jonghyun Park*[a]

This paper reports a multiscale controlled three-dimensional (3D) electrode structure to boost the battery performance for thick electrode batteries with $LiMn_{1.5}Ni_{0.5}O_{4\ as}$ cathode material, which exhibits a high areal capacity (3.5 mAh/cm^2) along with a high specific capacity (130 mAh/g). This excellent battery performance is achieved by a new concept of cell electrode fabrication, which simultaneously controls the electrode structure in a multiscale manner to address the key challenges of the material. Particles with ultrathin conformal coating layers are prepared through atomic layer deposition followed by a nanoscale-controlled, thermal diffusion doping. The particles are organized into a macroscale-controlled 3D hybrid-structure. This synergistic control of nano-/macro-structures is a promising concept for enhancing battery performance and its cycle life. The nanoscale coating/doping provides enhanced fundamental properties, including transport and structural properties, while the mesoscale control can provide a better network of the nanostructured elements by decreasing the diffusion path between. Electrochemical tests have shown that the synergistically controlled electrode exhibits the best performance among non-controlled and selectively-controlled samples, in terms of specific capacity, areal capacity, and cycle life.

Lithium-ion batteries (LIBs) are being used as the key energy storage in many applications.[1–3] In all applications, the important elements of LIBs that must be considered include power density, energy density, safety, cycle life, and cost. To meet these demands, it is urgent to optimize battery electrode structure, as much as new material development, because electrode structure significantly determines battery performance.[4] In particular, an optimized 3D structure can enhance a facile transport of ions by providing a short diffusion path with enhanced electrochemical reaction sites through a higher interface area, which has shown a huge potential for obtaining better battery performances.[3–6] In recent decades, the extrusion-based additive manufacturing processes have shown many advantages, as compared to other additive manufacturing technologies, due to the fact that they are inexpensive and flexible enough to fabricate more complex geometry designs, that can be applied to a wider selection of materials with a high mass loading.[7] For battery applications, the conventional cast-based process cannot achieve 3D-structured electrodes and, therefore, the additive manufacturing technique is a very promising method for fabricating 3D battery electrodes.[5,6,8–12] From the particle level, modification of the particle surface is an effective way to enhance performance. In particular, Atomic Layer Deposition (ALD) has emerged as one of the promising techniques for depositing a conformal ultrathin film on electrode materials. An ALD film can provide a uniform protection for the surfaces of particles against side reactions, as well as suppress the dissolution of transition metal and provide a longer cycle life.[13] Coating a conductive film using ALD will facilitate the kinetics of electrochemical reactions and improve the specific capacity of an electrode material.[14]

This paper details an innovative approach to boost battery performance via modifying the electrode structure at nano- and macro-scales. The proposed process integrates the ALD with annealing for particle surface treatment at the nano-level, and the extrusion-based additive manufacturing process controls and optimizes the electrode structure at the macro-level. This demonstrates a new possibility for fabricating battery electrodes, which has the potential for combining multiple technologies to control material architectures. This could lead to a transformational enhancement of key energy storage parameters that include capacity, energy density, and cycle life. The proposed approach is material-independent. In this study, LiMn1.5Ni0.5O4 (LMNO) is selected as the active material because LMNO has a potential of 4.7 V, providing it with a significant advantage over current battery materials. However, the ordered form of this material has poor ionic diffusivity, which results in lower cell performance than its disordered form. In its disordered form, ion diffusion is high, but it is prone to performance-degrading side reactions, such as oxygen loss, where side products of lithium, nickel, and oxygen are formed.[15,16] Naturally, this lowers the capacity of the cell, due to being inert for electrochemical reactions. This also creates a portion of manganese ions that, while partially able to act as an electrode material of 4 V, are prone to devolving into manganese ions that can dissolve in the electrolyte, causing an associated capacity loss. Also, mechanical strain results from volume change (6.3 % for LMNO) during the intercalation and degrades battery performance.[17]

[a] Dr. J. Li, Prof. J. Park
Department of Mechanical and Aerospace Engineering
Missouri University of Science and Technology
Rolla, MO, 65409, USA
E-mail: parkjonghy@mst.edu
[b] Y. Gao, Prof. X. Liang
Department of Chemical and Biochemical Engineering
Missouri University of Science and Technology
Rolla, MO, 65409, USA

Supporting information for this article is available on the WWW under https://doi.org/10.1002/batt.201800091

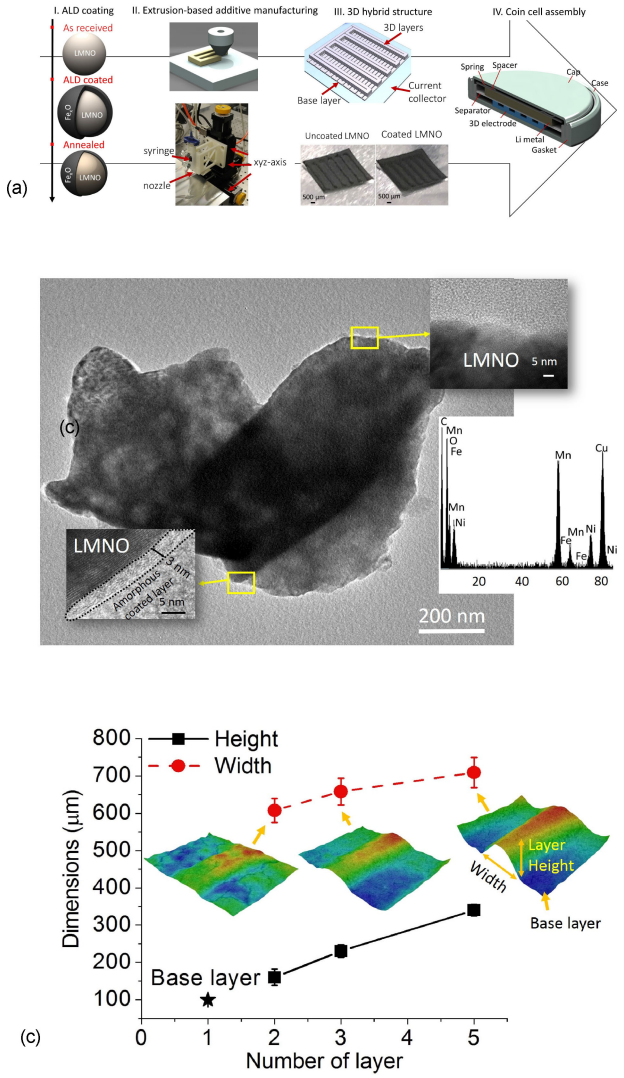

Figure 1. a) Procedure of the electrode fabrication via ALD coating and additive manufacturing, and comparison of material properties, b) TEM image of single coated particle, and c) heights and widths of printed structures as a function of number of layers.

As the first step (Figure 1a), the individual particles were coated with FeO_x by ALD, followed by an annealing process. The annealing processing after coating could be considered as doping the particles with FeO_x,[18] which might stabilize the active material in the electrolyte, and disorder the structure to improve battery performance.[18–20] Next, the pastes with particles (coated or non-coated) were extruded into a 3D hybrid structure (Figure S1) and tape casted as a conventional structure, respectively, and then assembled as a half-cell (Li foil anode) based on a coin cell design. To confirm the ALD coating layers on the LMNO particle surfaces, Transmission Electron Microscopy (TEM) was used for FeO_x coated LMNO particles followed by annealing. As shown in Figure 1b, the particles were partially coated with 3 nm FeO_x. This was because the coated FeO_x could be diffused inside the particles during annealing, which was also observed based on XRD analysis (Figure S2). Next, the viscosities of the coated and uncoated LMNO pastes were measured to identify the paste's behavior (Figure S3). In general, the two pastes were identical at the standoff condition ($\gamma = 0$) and the extrusion condition ($\gamma > 10^2$). Then, the 3D electrode thicknesses and widths of filaments as a function of layer numbers were measured as plotted in Figure 1c. These are 3D optical scanned images of one filament with different numbers of 3D layers. It was found that the thickness increased linearly with the increased number of layers, and the width slightly increased with more printed layers. This was because the extrusion-based fabrication methods suffer from gravitational forces when the aspect ratio (height/width) becomes high. In this case, the paste could merge slightly with the previous layer and then increase the total width of the 3D structure.

Four cases were compared, including uncoated LMNO with a conventional structure (noted as UC-Con), uncoated LMNO with a 3D hybrid structure (noted as UC-3D), coated LMNO with a conventional structure (noted as CO-Con), and coated LMNO with a 3D hybrid structure (noted as CO-3D). Figures 2a and 2b show the specific and areal capacity as a function of electrode thickness. The specific capacities of UC-Con samples were measured at different thicknesses from 30 to 170 μm. It was observed that the specific capacity decreased with the increasing electrode thickness. At 110 μm, the UC-Con could maintain a good performance with high specific capacity (100 mAh/g) and high areal capacity (0.9 mAh/cm^2). Then, this thickness (110 μm) was used as the basis for layer thickness; later, additional multiple numbers of 3D layers were printed on top of it. By utilizing the 3D structure, a higher capacity (> 100 mAh/g) could be maintained, even with a thicker thickness (230 μm). This was possible because of the short diffusion path with enhanced electrochemical reaction sites through higher interfacial area. Eventually, however, the capacity decreased as the electrode thickness increased further, where the 3D structures no longer helped. To compare the effect of ALD coating on battery performance, the CO-Con samples were fabricated at 50 and 110 μm, corresponding to the UC-Con samples, and the CO-3D were fabricated at the same thicknesses as the UC-3D samples. It was observed that (1) the coated samples could increase the specific capacity at any thickness considerably, regardless of the structures; and (2) the 3D hybrid structure could improve the performance at a thick electrode, regardless of the active materials.

Battery performance was compared at different C-rates (0.1 C, 0.2 C, 0.5 C, and 1 C), as shown in Figures 2c and 2d. The 3D structures (2.1 mAh/cm^2 and 1.9 mAh/cm^2) showed three time more areal capacity than that of conventional structure (0.6 mAh/cm^2 and 0.5 mAh/cm^2) at 0.1 and 0.2 C, respectively. The UC-3D showed less areal capacity at high C-rates (0.5 C and 1 C), but still approximately three times (0.9 mAh/cm^2 and 0.1 mAh/cm^2) more than that of UC-Con (0.3 mAh/cm^2 and 0.03 mAh/cm^2). By coating the LMNO materials, the conductivity and diffusivity of the electrode could be improved. As a result, the CO-3D (1.7 mAh/cm^2 and 1.2 mAh/cm^2) could keep a high areal capacity, and the CO-Con also showed a better performance (0.4 mAh/cm^2 and 0.3 mAh/cm^2) than that of UC-Con at high C-rates. Thus, the CO-3D could achieve the highest

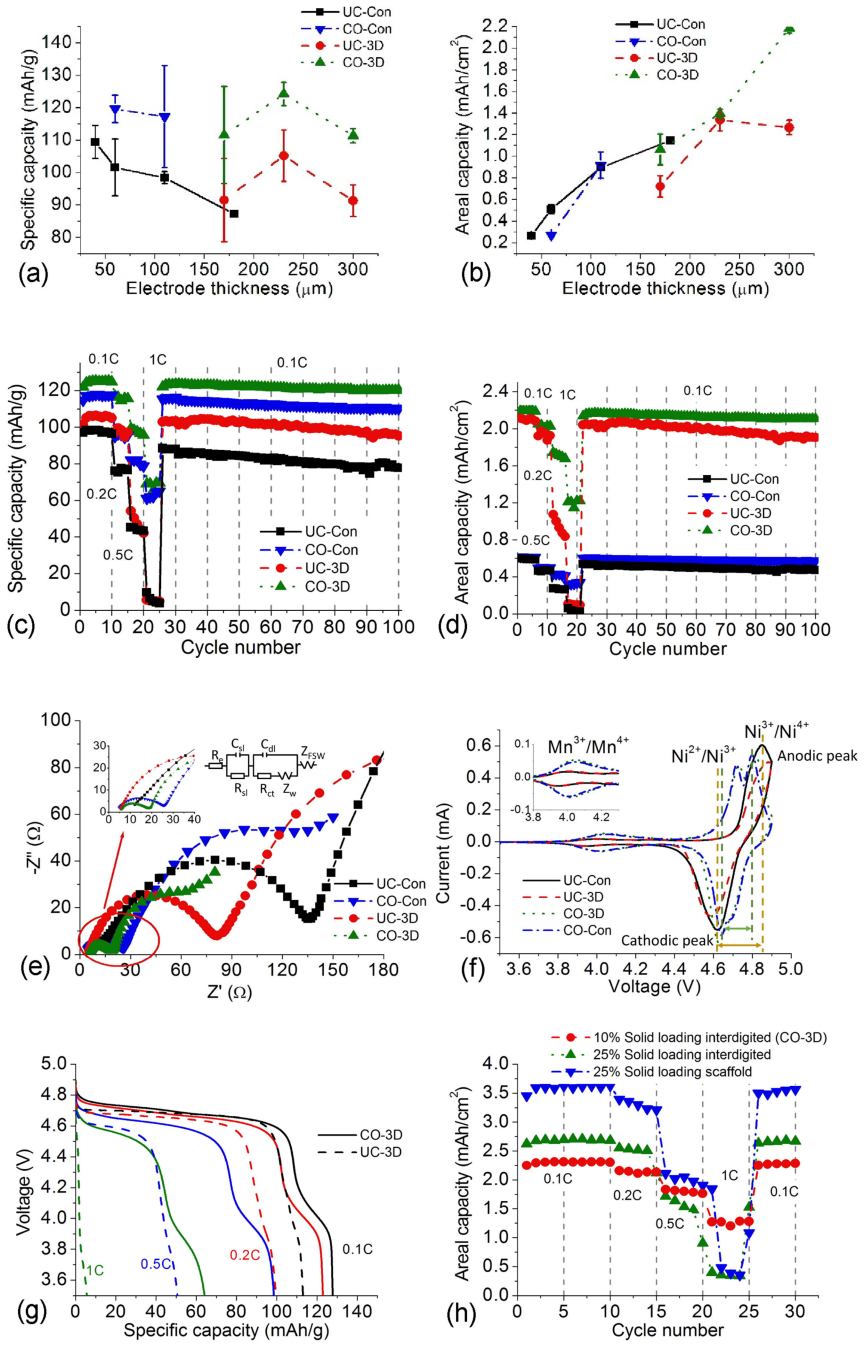

Figure 2. Comparison of the four cases in terms of a) specific capacity and b) areal capacity, cycling performance at difference C-rates of c) specific capacity and d) areal capacity, e) impedance analysis, f) cyclic voltammetry; g) voltage profile for CO-3D and UC-3D at different Crates, and h) comparison of coated samples with different 3D structures and different paste solids loadings.

areal capacity, compared to three other samples. In addition, after extra 60 cycles of charge/discharge with 0.1 C when the UC-Con sample lost 20% capacity (Figure S4), it was observed that all samples exhibited a steady degradation, and the capacity degradation rate could be reduced approximately 50% by coating, as CO-Con (0.07%/cycle) and CO-3D (0.04%/cycle), comparing to the uncoated samples as UC-Con (0.17%/cycle) and UC-3D (0.13%/cycle). This implied that the simultaneous control, including particle surface modification and shaping 3D structure of the electrode, could significantly boost battery performance.

To fully understand the electrochemical behavior of the four samples, an Electrochemical Impedance Spectrum (EIS) test was conducted. The original data was fitted by a circuit diagram model of $R_e(C_{sl}R_{sl})(C_{dl}R_{ct}Z_w)Z_{FSW}$. The Nyquist plots for the four samples are shown in Figure 2e. It was observed that all of the cells had a similar (7~10 Ω) ohmic resistance, but the semicircles of the samples in the 3D structure were smaller than those of the samples of conventional structures. In addition,

the coated samples had much smaller semicircles than those in the samples without ALD coating. Based on the fitted impedance parameters, the charge transfer resistance, R_{ct}, of the CO-3D had the smallest Rct (10.1 Ω) among the CO-Con (17.5 Ω), the UC-3D (66.7 Ω), and the UC-Con (98.4 Ω), indicating that the 3D structure and ALD coating could improve the inserting and de-inserting of lithium-ions.

In addition, the low and middle frequency regions of the impedance curves for coated and uncoated samples showed a difference, which suggested the reaction mechanism might have changed due to the doping. To characterize it, cyclic voltammetry tests were conducted with 0.025 mV/s. As shown in Figure 2f, the coated samples (green line range) showed a 40% smaller difference between the anodic and cathodic peaks than those of the uncoated samples (yellow line range), which suggested a smaller polarization and better conductivity of the coated samples. It was also observed that the coated samples had more significant $N^{i2+/4+}$ peaks at 4.5 to 4.8 V and $Mn^{3+/4+}$ at 3.6 to 4.3 V than the uncoated samples did, which indicated increased amounts of $Ni^{2+/4+}$ and $Mn^{3+/4+}$ redox couples.[18] The peak of the $Ni^{2+/4+}$ redox couple is known as one peak for an ordered LMNO structure, while the Ni exhibits two-step reactions, including $Ni^{3+/4+}$ and $Ni^{2+/3+}$ for a disordered LMNO structure. A peak of a $Mn^{3+/4+}$ redox couple of around 4.0 V is also commonly seen in a disordered LMNO structure.[20,21] In addition, there was no significant difference in the CV responses between the samples of a conventional structure and a 3D structure, which was reasonable, since that structure did not affect the chemical properties. The results from CV measurement were consistent with the voltage profiles, as shown in Figure 2g. Due to the plateau, at about 4.6 to 4.8 V, and clear changes at around 4.0 V, the specific capacities of the coated samples increased nearly 20 mAh/g at low C-rates (0.1 and 0.2 C) and considerably increased the performance at high C-rates (0.5 and 1 C).

To further enhance the mass loading, the paste solid loading (SL) can be increased, or a denser electrode structure can be constructed. For this, two samples with coated particles at 230 µm electrode thickness were fabricated with (1) 25% solid loading paste with interdigitated structure and (b) 25% solid loading paste with a grid structure on top of the base layer (Figure 2h). Those samples when compared to the 10% SL paste printed samples (used in this study as CO-3D), demonstrated that the areal capacity could be improved by over 25% to 75% to obtain a high areal capacity. This result exhibited a higher areal capacity (3.48 mAh/cm^2) for LMNO than the records[22–24] in recent five years, due to its high active material mass loading (approximately 25 mg/cm^2) and high specific capacity (approximately 135 mAh/g) which benefited from the 3D structure and ALD coating (Figure 2h and S5).

The Scanning Electron Microscopy (SEM) images of the UC-3D and CO-3D (as-printed and after cycling) were compared to study the effect of ALD coating on particle morphology, as shown in Figure 3. Comparing fresh samples of uncoated and coated electrodes (Figure 3a and 3b), the coated particles showed a rougher surface than the uncoated samples did, which was due to the coated FeO_x layer partially diffused into the particle, as observed in TEM, while the remaining coated layers were crystallized. To confirm the surface morphology of the uncoated and coated samples, SEM images were taken for the particle specimens (Figure S6). It was observed that the particle samples had the same morphology as the electrode samples and, it was also observed that the uncoated sample surface was smooth with sharp boundaries, while the coated sample's surface was rough and covered with small crystal structures. As shown in Figure 3c, the uncoated samples, after cycling, showed crack formation on the surfaces of the particles (red circle) and the particle grain boundaries had become dull, as compared to that of fresh particles, due to the dissolution of active materials. In contrast, the coated samples (Figure 3d) did not show any crack formation and the particle surfaces had no significant changes. These observations indicated that the coated surfaces could protect battery active material from mechanical and chemical degradation.

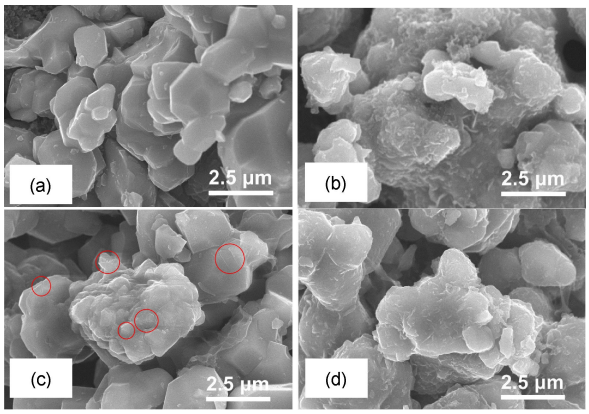

Figure 3. SEM images of as-printed electrode samples of (a) uncoated and (b) coated, and cycled electrode samples of (c) uncoated and (d) coated.

In summary, a novel fabrication approach that utilizes the advantages of a 3D structure and ALD coated particles is proposed to boost battery performance with a thick electrode. By combining these two technologies, the battery performance (i.e., CO-3D compared to UC-Con) can be boosted 1.3 times more at low C-rates (0.1 C and 0.2 C), and 7 times more at high C-rates, in terms of specific capacity; 3.5 times more at low C-rates (0.1 C and 0.2 C), and 24 times more at high C-rates in terms of areal capacity. This is the highest record for LMNO material and the superiority of this proposed approach can be extended to different materials systems. This multiscale controlled electrode fabrication for high performance LIBs offers a new avenue for future design and fabrication of energy storage devices.

Experimental Section

ALD Coating: The FeOx ALD was performed in a fluidized bed reactor.[25] In a home-built fluidized-bed ALD reactor, FeOx ALD was applied on LMNO primary particles at 450 °C using ferrocene (Alfa Aesar) and oxygen as precursors. The ferrocene was heated at 115 °C in a bubbler, and all the feed lines were kept at ~120 °C to avoid any condensation. N2 was applied as either carrier gas of

ferrocene or flush gas. Before FeOx ALD reaction, the fluidization gas flow rate was determined. A typical FeOx ALD cycle consisted of (1) 780 s dose of ferrocene with 9 sccm N2 flow, (2) 600 s N2 flush at 9 sccm to remove unreacted precursors and any by-products, (3) 10 s purge to evacuate the reactor chamber, (4) 800 s dose of oxygen at 10 sccm, (5) 600 s N2 flush at 9 sccm to remove any by-products and residual oxygen, and (6) 10 s purge to evacuate the reactor chamber. 50 cycles of FeOx ALD was applied. The growth rate of FeOx was comparable to our previous results.

Material Characterization: The FeO_x films were observed and verified by using the TEM (FEI Tecnai F20). The morphologies of the printed samples were characterized with an SEM (Hitachi S4700) by using secondary electrons at 20 kV accelerating voltage.

LMNO Paste Preparation: The LMNO pastes, with uncoated or ALD coated LMNO particles, were prepared by mixing 80 wt.% LMNO (NEI Corporation) with 10 wt.% carbon black (CB, Alfa Aesar), 10 wt.% polyvinylidene fluoride (PVDF, Sigma-Aldrich), and N-Methyl-2-pyrrolidone (NMP, Sigma-Aldrich) for different solid loadings. The paste rheology was measured by a viscometer (Brookfield model HB) at the room temperature.

Electrode Fabrication: An extrusion-based additive manufacturing system was used to extrude the paste into a 3D structure. An aluminium foil piece was fixed on a substrate, prior to printing, which was then used as a current collector after assembly. The extrusion-based additive manufacturing system was a home-built system consisting of a motion subsystem, a hot plate, and an extrusion device. The paste was loaded into a 5cc plastic syringe with a 200 μm nozzle (EFD Inc.), and extruded with 5 psi extrusion pressure onto the substrate that moved along the XY-axes. First, a base layer was printed to cover the current collector as a conventional laminated structure. Next, a patterned structure was printed on top of the base layer to increase the specific surface area. For comparison, the conventional laminated structure was fabricated via the tape casting and the same paste was used as the additive manufacturing method. After fabrication, the electrodes were dried in a vacuum oven at 120 °C overnight to remove the remaining NMP.

Battery Assembly: A CR2032 coin cell (Wellcos Corp) was used to assemble a battery in a glove box. The battery used LMNO as the cathode, Li foil (Alfa Aesar) as an anode, PP/PE/PP membrane (Celgard) as a separator, and filled with liquid electrolyte 1 M LiPF6 EC:DMC 1 : 1 (Sigma-Aldrich).

Electrochemical Characterization: The electrochemical behaviours of the batteries were measured from 3.5 V to 4.9 V by using a battery testing station (IVIUMnSTAT). The specific capacities and areal capacities were measured under a 0.1 C rate, and then the cycling performance was conducted under 0.1 C, 0.2 C, 0.5 C, and 1 C per five cycles based on the theoretical capacity 147mAh/g and the masses of the electrodes. The batteries' impedances were measured via EIS at 4.7 V open circle voltage with 1×10^{-3}% current amplitude variation from 1 MHz to 5×10^{-2} Hz.

Acknowledgements

The authors gratefully acknowledge the financial support from National Science Foundation Awards (CMMI-1563029, CBET-1510085)

Conflict of Interest

The authors declare no conflict of interest.

Keywords: atomic layer deposition · lithium-ion batteries · materials science · multiscale controlled structure · thick electrode

[1] B. Scrosati, J. Garche, *J. Power Sources* **2010**, *195*, 2419–2430.
[2] M. Armand, J. M. Tarascon, *Nature* **2008**, *451*, 652.
[3] T. S. Arthur, D. J. Bates, N. Cirigliano, D. C. Johnson, P. Malati, J. M. Mosby, E. Perre, M. T. Rawls, A. L. Prieto, B. Dunn, *MRS Bull.* **2011**, *36*, 523.
[4] K. G. Gallagher, S. E. Trask, C. Bauer, T. Woehrle, S. F. Lux, M. Tschech, P. Lamp, B. J. Polzin, S. Ha, B. Long, *J. Electrochem. Soc.* **2016**, *163*, A138.
[5] J. Li, M. C. Leu, R. Panat, J. Park, *Mater. Des.* **2017**, *119*, 417–424.
[6] S. Ferrari, M. Loveridge, S. D. Beattie, M. Jahn, R. J. Dashwood, R. Bhagat, *J. Power Sources* **2015**, *286*, 25–46.
[7] I. Gibson, D. W. Rosen, B. Stucker, *Additive manufacturing technologies*, Springer **2010**.
[8] D. S. Engstrom, B. Porter, M. Pacios, H. Bhaskaran, *J. Mater. Res.* **2014**, *29*, 1792–1816.
[9] K. Fu, Y. Wang, C. Yan, Y. Yao, Y. Chen, J. Dai, S. Lacey, Y. Wang, J. Wan, T. Li, Z. Wang, *Adv. Mater.* **2016**, *28*, 2587–2594.
[10] J. Li, X. Liang, F. Liou, J. Park, *Sci. Rep.* **2018**, *8*, 1846.
[11] S. H. Kim, K. H. Choi, S. J. Cho, S. Choi, S. Park, S. Y. Lee, *Nano Lett.* **2015**, *15*, 5168–5177.
[12] M. S. Saleh, J. Li, J. Park, R. Panat, *Additive Manufacturing* **2018**, *23*, 70–78.
[13] X. Zhang, I. Belharouak, L. Li, Y. Lei, J. W. Elam, A. Nie, X. Chen, R. S. Yassar, R. L. Axelbaum, *Adv. Energy Mater.* **2013**, *3*, 1299–1307.
[14] Y. Gao, R. L. Patel, K. Y. Shen, X. Wang, R. L. Axelbaum, X. Liang, *ACS Omega*, **2018**, *3*, 906–916.
[15] K. Kim, Y. Kim, E. S. Oh, H. C. Shin, *Electrochim. Acta* **2013**, *114*, 387–393.
[16] D. S. Lu, L. B. Yuan, J. L. Li, R. Q. Huang, J. H. Guo, Y. P. Cai, *J. Electroanal. Chem.* **2015**, *758*, 33–38.
[17] S. Kuppan, Y. Xu, Y. Liu, G. Chen, *Nat. Commun.* **2017**, *8*, 14309.
[18] N. H. Vu, J. C. Im, S. Unithrattil, W. B. Im, *J. Mater. Chem. A* **2018**, *6*, 2200-2211.
[19] J. Huang, H. Liu, N. Zhou, K. An, Y. S. Meng, J. Luo, *ACS Appl. Mater. Interfaces* **2017**, *9*, 36745–36754.
[20] W. Liu, Q. Shi, Q. Qu, T. Gao, G. Zhu, J. Shao, H. Zheng, *J. Mater. Chem. A* **2017**, *5*, 145–154.
[21] F. M. Vitucci, A. Paolone, O. Palumbo, G. Greco, L. Lombardo, M. Köntje, A. Latini, S. Panero, S. Brutti, *J. Am. Ceram. Soc.* **2016**, *99*, 1815–1822.
[22] M. Bini, P. Boni, P. Mustarelli, I. Quinzeni, G. Bruni, D. Capsoni, *Solid State Ionics* **2018**, *320*, 1–6.
[23] G. Gabrielli, M. Marinaro, M. Mancini, P. Axmann, M. Wohlfahrt-Mehrens, *J. Power Sources* **2017**, *351*, 35–44.
[24] S. Solchenbach, M. Wetjen, D. Pritzl, K. U. Schwenke, H. A. Gasteiger, *J. Electrochem. Soc.* **2018**, *165*, A512–A524.
[25] X. Liang, L. F. Hakim, G. D. Zhan, J. A. McCormick, S. M. George, A. W. Weimer, J. A. Spencer, K. J. Buechler, J. Blackson, C. J. Wood, J. R. Dorgan, *J. Am. Ceram. Soc.* **2007**, *90*, 57–63.

Manuscript received: September 12, 2018
Accepted manuscript online: October 1, 2018
Version of record online: November 14, 2018